12272 *Biochemistry* **2009,** *48,* 12272–12282
DOI: 10.1021/bi901521d

BIOCHEMISTRY
including biophysical chemistry & molecular biology
Article

Computational Studies of Ammonia Channel Function in Glutamine 5′-Phosphoribosylpyrophosphate Amidotransferase[†]

Xiang S. Wang,[‡] Adrian E. Roitberg, and Nigel G. J. Richards*

Department of Chemistry, University of Florida, Gainesville, Florida 32611-7200, and Quantum Theory Project, University of Florida, Gainesville, Florida 32611-8435. [‡]Present address: Division of Medicinal Chemistry and Natural Products, University of North Carolina School of Pharmacy, Beard Hall, Chapel Hill, NC 27599-7360.

Received August 30, 2009; Revised Manuscript Received November 17, 2009

ABSTRACT: Glutamine 5′-phosphoribosylpyrophosphate amidotransferase (GPATase) catalyzes the synthesis of 5′-phosphoribosylamine in a reaction that involves the translocation of ammonia along an intramolecular tunnel linking the two active sites of the enzyme. We now report a locally enhanced sampling (LES) strategy for modeling ammonia transfer between the active sites of *Escherichia coli* GPATase in its active conformation. Our calculations demonstrate that the ammonia channel in GPATase is best regarded as a "pipe" through which ammonia travels in the absence of an external "driving" potential. This combined LES/PMF computational approach, which offers a straightforward alternative to steered molecular dynamics simulations in studies of substrate channeling, also provides new insights into the molecular basis of the reduced ammonia transfer efficiency exhibited by the L415A GPATase mutant.

Glutamine-dependent amidotransferases transfer nitrogen from the side chain of L-glutamine to various electrophilic acceptors (*1*, *2*). These enzymes play a critical role in the biosynthesis of cofactors (*3*−*5*), purines (*6*), pyrimidines (*7*), amino acids (*8*−*11*), and amino sugars (*12*). High-resolution crystal structures are now available for 10 amidotransferases, which all show, or at least suggest, the presence of intramolecular tunnels linking multiple active sites in each enzyme (*13*−*22*). Although it is generally accepted that ammonia is translocated through the protein during catalytic turnover, questions concerning structure−function relationships in these structurally disparate tunnels and the molecular mechanisms that coordinate catalytic activity in the separate active sites of each amidotransferase remain (*23*−*25*).

To date, experimental assays have provided relatively limited answers to questions about the relationship between molecular structure and tunnel function (*26*−*30*). Several groups have therefore turned to computational simulation as a strategy for elucidating the dynamic and energetic details of ammonia translocation (*31*−*34*). For example, work employing "steered" molecular dynamics (SMD)[1] protocols gave valuable insights into how the tunnel in imidazole glycerol phosphate synthase might discriminate among ammonia, ammonium ion, and water in the translocation process (*31*). These studies also resulted in new hypotheses concerning the molecular interactions involved in coordinating active site chemistry, which were subsequently confirmed by experimental measurements (*35*, *36*). More recently, SMD studies have identified the role of interdomain orientation and substrate binding in tunnel formation and ammonia translocation in *Escherichia coli* glucosamine-6-phosphate synthase (*33*). The use of long time scale, unconstrained molecular dynamics (MD) simulations for modeling the movement of ammonia through the small subunit of carbamoyl phosphate synthase has also been reported (*34*). On the other hand, both of these approaches have some limitations, such as the need to generate sufficient trajectories when using SMD calculations to determine free energies (*37*). Perhaps more importantly, the ammonia molecule may become "trapped" in local energy minima that preclude its motion through the protein over easily accessible time scales when MD simulations are employed that do not include a biasing potential.

As an alternative to existing methods for studying the energetics of ammonia transfer in glutamine-dependent amidotransferases, we now report a computational strategy that combines locally enhanced sampling (LES) (*38*, *39*) and potential of mean force (PMF) calculations (*40*, *41*), which is similar to that used to model ligand dissociation from proteins, such as nuclear hormone receptors (*42*, *43*). In the LES method, N copies of ammonia are placed within the protein, which interact with the protein as a mean field even though they do not interact with each other. As explained elsewhere (*44*), LES has two advantages in simulating small molecule diffusion in proteins; more ligands explore their accessible conformational space, and conformational barriers to ligand diffusion are lowered by a factor of $1/N$. The LES protocol therefore provides a straightforward method for generating an "unbiased" trajectory for ammonia translocation within the tunnel, which can then be used with subsequent

[†]This work was supported by the Chiles Endowment Biomedical Research Program of the Florida Department of Health.

*To whom correspondence should be addressed: Department of Chemistry, Box 117200, University of Florida, Gainesville, FL 32611-7200. Phone: (352) 392-3601. Fax: (352) 846-2095. E-mail: richards@qtp.ufl.edu.

[1]Abbreviations: SMD, steered molecular dynamics; MD, molecular dynamics; LES, locally enhanced sampling; PMF, potential of mean force; GPATase, glutamine 5′-phosphoribosylpyrophosphate amidotransferase; PRPP, 5′-phosphoribosylpyrophosphate; WT, wild type; cPRPP, 1α-pyrophosphoryl-2α,3α-dihydroxy-4β-cyclopentanemethanol-5-phosphate; DON, 6-diazo-5-oxo-L-norleucine; NVT, simulation for which the number of atoms, volume, and temperature are constant; WHAM, weighted histogram analysis method; rms, root-mean-square; PDB, Protein Data Bank.

 Published on Web 11/18/2009

Scheme 1: Reaction Catalyzed by GPATase

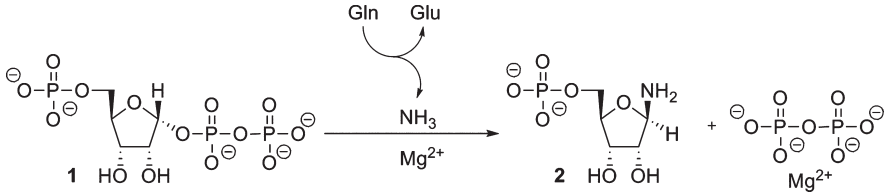

PMF calculations to provide quantitative information about the free energy of ammonia as it moves through the amidotransferase.

Our initial application of the LES/PMF strategy has been in studying ammonia transfer in glutamine 5′-phosphoribosylpyrophosphate amidotransferase (GPATase), the enzyme that catalyzes the conversion of 5′-phosphoribosylpyrophosphate (PRPP) **1** into 5′-phosphoribosylamine **2** (Scheme 1) (*14*, *45*). There is a substantial amount of structural and kinetic data for wild-type (WT) GPATase, and a series of site-directed GPATase mutants have been prepared in which ammonia translocation takes place with altered efficiency (*28*, *47*). A number of questions remain, however, concerning the details of ammonia channeling in the active conformation of GPATase that have not been addressed by experiment or computation. These include whether tunnel residues create a potential that "drives" enzyme-bound ammonia from the N- to C-terminal active site, the nature of dynamical motions in the protein during ammonia channeling, and the structural features that coordinate active site activities. Our LES/PMF simulations not only demonstrate that the 20 Å long channel linking the two active sites in GPATase (*14*) is best regarded as a "pipe" through which ammonia travels without any external electrostatic or steric driving force but also provide a dynamical explanation for the observed behavior of a GPATase mutant in which ammonia leaks from the protein into aqueous solution (*28*).

MATERIALS AND METHODS

Constructing a Model of Catalytically Active GPATase. The crystal structure of *E. coli* GPATase (PDB entry 1ECC) in a complex with cPRPP **3** (Figure 1) (*14*), a nonhydrolyzable analogue of PRPP substrate **1** (*48*, *49*), was used as the starting point for our computational studies. In this crystal structure, the side chain of Cys-1 is covalently modified by 6-diazo-5-oxo-L-norleucine **4**, a reactive analogue of L-glutamine (Figure 1) (*50*). The presence of these ligands allowed us to model the active form of GPATase containing both the γ-glutamylthioester (NTNG) **5** and bound PRPP **1** that are present when ammonia is released from glutamine and travels through the channel to react with PRPP in the synthase site. Importantly, functional groups on the γ-glutamylthioester were positioned to make noncovalent interactions with residues that are conserved throughout the glutaminase domains of the class II amidohydrolase domain (Figure 2) (*51*, *52*), as observed for the C1A mutant of *E. coli* asparagine synthetase B complexed with glutamine and AMP (*15*). Hydrogen atoms were added to the initial thioester−PRPP−GPATase model and crystallographic waters using the HBUILD module of the CHARMM software package (*53*), and the initial structure was energy minimized in vacuo using an adopted-basis Newton−Raphson algorithm, with positional restraints (1 kcal mol^{-1} $Å^{-2}$) imposed on heavy atoms defining the enzyme main chain, PRPP, and the γ-glutamylthioester intermediate.

Force Field Parametrization. All energy minimization, LES, and PMF calculations were performed using the CHARMM force field (PARAM27). Standard procedures (*54*−*56*) were employed to obtain empirical parameters for γ-glutamylthioester intermediate **5** and PRPP **1** (Tables S1−S5 of the Supporting Information) using calculations on model compounds *S*-methyl thioacetate (SMTA) **6** and tetrahydrofuran phosphoric acid (THFP) **7**, respectively (Figure 1).

LES Simulations. In the initial set of gas-phase LES simulations, 50 (N) copies of NH_3 molecules or ammonium ions (H_4N^+) were initially positioned at the N-terminal end of the channel in the geometry-optimized thioester−PRPP−GPATase model using the REPLICA facility in CHARMM. The nitrogen atoms of all copies were placed 1.48 Å from the thioester carbon along the vector defined by the C−N bond of the likely tetrahedral precursor to the thioester (*40*, *44*, *57*). Although all ammonia molecules occupy the same point in coordinate space, no interactions between copies are included in the potential energy function describing the system (*58*), and partial charges and Lennard-Jones parameters for atoms in each ammonia or ammonium ion are scaled by a factor of $1/N$.

The LES protocol was initially employed to obtain an equilibrium distribution of ammonia within the thioester−PRPP−GPATase model in the absence of a solvation potential. Thus, the initial structure was gradually heated to 300 K (reassignment of atomic velocities rather than by coupling to a temperature bath) over a period of 6 ps while the same restraints were maintained as employed in the energy minimization. An NVT MD simulation was then performed to equilibrate the thioester−PRPP−GPATase model at 300 K for a period of 20 ps, during which time the harmonic constraints (initially 1 kcal mol^{-1} $Å^{-1}$) were gradually eliminated. Subsequent production LES calculations at 300 K were performed for times of up to 200 ps in the same NVT ensemble, using the Nosé-Hoover method for temperature scaling (q_{ref} = 100.0) (*59*, *60*). Atomic coordinates and velocities were updated by the Verlet method (dt = 2 fs); covalent bonds to hydrogen were fixed by the SHAKE algorithm (*61*), and a distance-dependent dielectric constant ($\varepsilon = r$) was used in calculating the electrostatic energies. Nonbonded cutoffs of 13 and 9−13 Å were employed for electrostatic and dispersion interactions, respectively.

In a second series of simulations, aimed at evaluating the effects of solvent on the LES calculations, a sphere of equilibrated TIP3P water molecules (radius of 24 Å) (*62*), centered about the middle of the ammonia tunnel, was placed around the energy-minimized thioester−PRPP−GPATase−NH_3 model structure. Solvent molecules within 2.5 Å of non-hydrogen protein atoms or crystallographic waters were removed, and the resulting system was modeled as three concentric spherical shells. In the central region (radius of 20 Å), all atoms were allowed to move in the LES simulation without any restraints, while the motions of protein atoms and water molecules in the central "buffer" region (outer radius of 24 Å) were governed by Langevin equations of

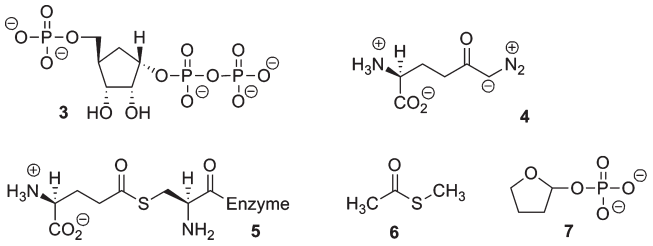

FIGURE 1: Chemical structures for compounds mentioned in the text, including γ-glutamylthioester intermediate **5**.

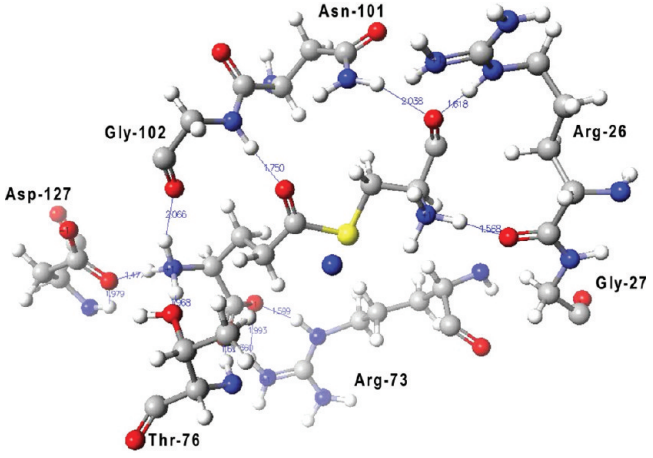

FIGURE 2: Model of γ-glutamylthioester intermediate **5** in the N-terminal, glutaminase active site of the thioester−PRPP−GPATase complex, showing hydrogen bonding interactions (blue lines) with conserved residues Arg-26, Gly-27, Arg-73, Thr-76, Asn-101, Gly-102, and Asp-127. The isolated blue sphere indicates the initial position of the nitrogen atom of the ammonia copies in the N-terminal site. Atom coloring: C, black; H, white; N, blue; O, red; S, yellow. This structure was visualized using CAChe Worksystem Pro version 6.5 (Fujitsu America Inc., Beaverton, OR).

motion, with friction coefficients of 80 and 62 ps^{-1}, respectively (*63*). Protein atoms in this buffer region were also constrained by a harmonic restoring force (1 kcal mol^{-1} $Å^{-2}$). Finally, protein atoms located in the outer, reservoir boundary shell (more than 24 Å from the system center) were fixed at their initial positions and retained in the potential energy function to provide a static reaction field about the dynamic region. Water molecules were held within the outer simulation sphere using a deformable stochastic boundary potential (*64*). The LES protocol used for studying the distribution of ammonia copies within the intramolecular tunnel was identical to that described above for the gas-phase modeling study.

Control simulations were also performed for the two systems, using protocols identical to those outlined above, by placing 50 ammonia copies (i) in the synthase site or (ii) at the center of the tunnel. In additional control studies, 10 ammonia copies were initially placed in the glutaminase site, with partial charges and Lennard-Jones parameters for atoms in each ammonia molecule being scaled by $^1/_{10}$ in the resulting LES simulations. Calculations on (i) the behavior of ammonium ions in the tunnel of the thioester−PRPP−GPATase complex and (ii) the motions of ammonia molecules in the L415A GPATase mutant employed equilibration and simulation protocols identical to those described above.

Umbrella Sampling Calculations. Starting coordinates for these simulations were derived from the structure obtained after 28 ps of the solvated LES trajectory in which the ammonia copies were distributed throughout the length of the intramolecular tunnel (Figure 3A). Then a series of structures were generated for use in subsequent free energy calculations via deletion of all but one of the ammonia (or ammonium ion) copies in the reference thioester−PRPP−GPATase snapshot. The free energy difference for the single bound ligand at adjacent locations in the LES trajectory snapshot was computed by "umbrella sampling" using a harmonic biasing potential [$U(\delta) = K(\delta - \delta_o)^2$] to hold the ammonia nitrogen atom at a specific location in the protein during each MD simulation (*41*, *65*). Here, K and δ are a biasing force constant and a "translation coordinate" (defined as the distance between the ammonia nitrogen and the carbonyl carbon of the thioester bonded to the Cys-1 side chain), respectively. Prior to umbrella sampling simulations, the thioester−PRPP−GPATase−NH_3 structure at each "window" was energy minimized using a distance restraint to maintain the distance δ at the appropriate value relative to the carbonyl carbon of the thioester. The system was equilibrated at 300 K (10 ps) before the umbrella sampling was performed using MD simulation parameters identical to those used in the LES calculations. The minimum of the biasing potential was shifted along δ by 0.5 Å in each window, and the distribution of δ values, $\rho(\delta)$, for each trajectory was determined using bins 0.1 Å in width. Calculations of the potential of mean force, $W(\delta)$, employed the following expression:

$$W(\delta) = -k_B T \ln[\rho(\delta)] - U(\delta) + C_i$$

where k_B is the Boltzmann constant, T is the temperature, $U(\delta)$ is the biasing potential, and C_i is a constant that is different for each window. The $(N+1)$th window began from the far end of the previous (Nth) window along the translational coordinate δ, but with an overlap of 32.5% in the distance coverage (*65*). To ensure complete sampling across the entire reaction coordinate, especially at overlapping regions, the value of biasing constant K (10.0 kcal mol^{-1} $Å^{-2}$) was optimized for individual windows on the basis of (i) the plot of free energy and (ii) the variation in dynamic δ_o versus time. The final set of PMF energies was calculated using the Weighted Histogram Analysis Method (WHAM) (*66*), as implemented in WHAM version 2.0.2.

Analysis of Tunnel Structure and Properties. Cavities within the initial model of *E. coli* GPATase (PDB entry 1ECC) and "snapshot structures" formed during the LES simulations were identified using VOIDOO (*67*). The accessible volume was computed using a probe radius of 1.4 Å and an atomic "fattening" factor of 1.1, with a grid shrink factor of 0.9 being employed in cavity refinement procedures. The cavities were visually rendered in O (*68*), and plot files were created using MAPMAN (*69*). The electrostatic potentials at the surface of the intramolecular tunnel were computed from the Poisson−Boltzmann equation, using the algorithms implemented within GRASP (*70*) and partial charges on all atoms as assigned in the CHARMM force field (*54*). The molecular surface of the tunnel was constructed from the van der Waals radii of atoms in residues Tyr-74, Thr-76, Arg-188, Phe-254, Glu-255, Tyr-258, Phe-259, Phe-334, Ile-335, Gly-406, and Ile-407.

RESULTS AND DISCUSSION

Delineating the Ammonia Translocation Pathway in WT GPATase Using Locally Enhanced Sampling Simulations. To investigate the nature of ammonia translocation between the two active sites in GPATase, including the role played by the

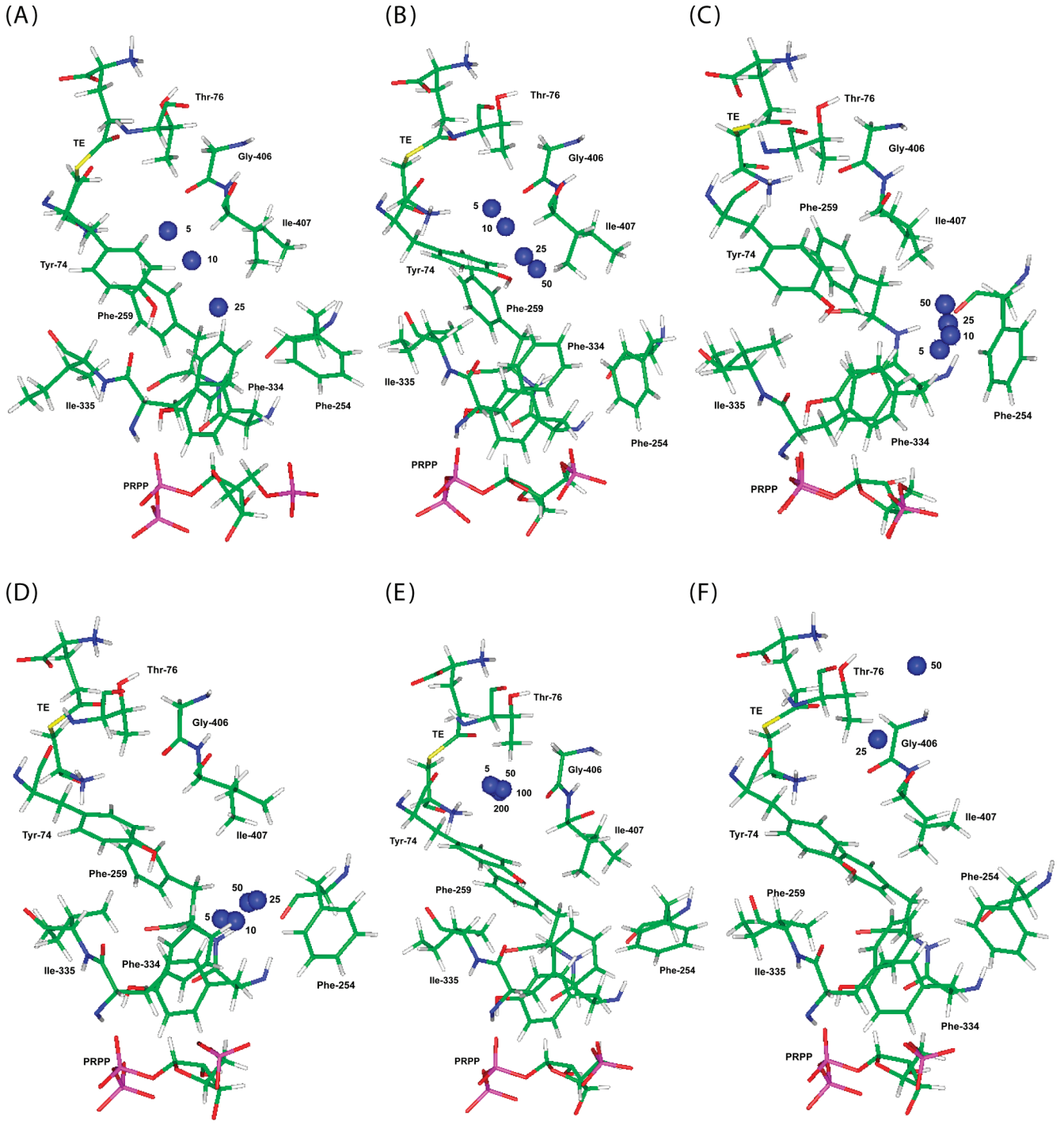

FIGURE 3: Visualizations of the distribution of ammonia or ammonium ion copies as a function of time during the LES simulations. (A) Gas-phase LES simulation for 50 ammonia copies starting in the glutaminase site (top). (B) Stochastic boundary LES simulation for 50 ammonia copies with an initial position identical to that shown in panel A. (C) Stochastic boundary LES simulation for 50 ammonia copies starting in the synthase site (bottom). (D) Stochastic boundary LES simulation for 50 ammonia copies initially placed midway between the active sites. (E) Stochastic boundary LES simulation for 10 ammonia copies with the initial position identical to that of the LES simulation shown in panel A. (F) Stochastic boundary LES simulation for 50 ammonium ion (NH_4^+) copies with a starting position identical to that of the LES simulation shown in panel A. In all images, the protein is oriented so that the glutaminase site in the N-terminal domain is at the top, and the isolated blue spheres represent the location of the center of mass for the ammonia copies in the tunnel at various times (picoseconds) as indicated by the adjacent number. Atom coloring: C, green; H, white; N, blue; O, red; P, pink; S, yellow.

enzyme residues defining the surface of the observed tunnel, we first needed to identify the path along which ammonia might move through the protein. We were also interested in examining whether the tunnel structure was formed as a consequence of ammonia dynamics within the protein, especially given current interest in the functional role of dynamical motions in enzymes (*71*−*73*).

We therefore built a model of the GPATase−thioester−PRPP−NH_3 complex, based on the crystal structure of the DON-modified *E. coli* enzyme complexed with cPRPP **3** (*14*), in which 50 ammonia copies were placed at the same initial position within the N-terminal, glutaminase site. The behavior of this system was first evaluated using a gas-phase LES simulation with the putative ammonia tunnel being devoid of water

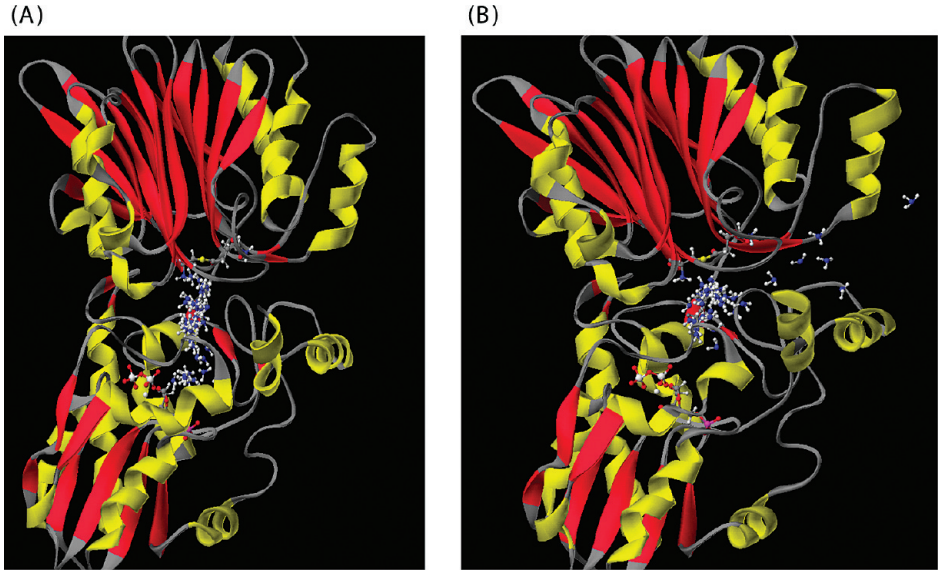

FIGURE 4: Distribution of ammonia copies within the tunnel linking the two active sites. (A) Snapshot of the wild-type *E. coli* GPATase−thioester−PRPP complex after 28 ps in the stochastic boundary LES simulation. Note that the ammonia copies are distributed along the complete extent of the tunnel. (B) Snapshot of the L415A GPATase mutant−thioester−PRPP complex after 39 ps, showing the leakage of ammonia into bulk solution. In the cartoon of the protein, α-helices and β-strands are colored yellow and red, respectively. The glutaminase site is located at the top of the image. Ammonia copies, γ-glutamylthioester intermediate **5**, and PRPP are shown as "ball-and-stick" representations. Atom coloring: C, gray; H, white; N, blue; O, red; P, orange; S, yellow.

molecules. Even though no external forces were applied, the 50 ammonia copies moved away from their original location and became evenly distributed within the protein throughout the tunnel cavity proposed on the basis of X-ray crystallography (see below). The time dependence of this distribution could be visualized by plotting the location of the center of mass for the 50 nitrogen atoms in the ammonia molecules (Figure 3A). At times longer than 25 ps, the ammonia copies completely occupied the tunnel (Figure 4A). Longer simulation times (> 100 ps) were precluded by the fact that ammonia molecules leaked from the C-terminal domain as a result of nonproductive collisions with the bound substrate. A series of "control" calculations were then performed to evaluate the effect of changing the initial conditions on the observed distribution of ammonia copies throughout the tunnel. For example, placing the 50 copies at initial locations (i) within the C-terminal synthase site or (ii) at the approximate midpoint of the tunnel gave distributions of ammonia copies essentially identical to that observed when the copies were placed initially in the N-terminal, glutaminase site (data not shown). The observation that the ammonia copies become distributed evenly through the intramolecular space, in a manner independent of their initial position, suggests the absence of a free energy gradient along the tunnel, which might arise from either local electrostatic properties or asymmetry in the tunnel radius, to promote migration of ammonia from the N-terminal glutaminase domain to the C-terminal synthase site of the enzyme. This conclusion also appears consistent with the calculated electrostatic potential of the van der Waals surface of the residue side chains within the interior of the tunnel (Figure 5).

The effect of protein solvation on the equilibrium distribution of ammonia copies within the tunnel was next investigated using a stochastic boundary potential in which a shell of water molecules, centered on the tunnel, was placed about the GPATase−thioester−PRPP−NH_3 complex. A series of LES simulations were performed on this system with the ammonia copies identically placed to the cognate gas-phase calculations. As before, when started in the glutaminase site, the ammonia molecules became distributed throughout the tunnel region, albeit after a longer time (40 ps) (Figure 3B). Placing the ammonia copies initially in the synthase site and at the tunnel midpoint also resulted in the "center of mass" for the ligands becoming located at the center of the tunnel at times of up to 100 ps (panels C and D of Figure 3, respectively). The extended times required for equilibration of the ammonia copies in these stochastic boundary simulations result from both the presence of the solvent and the constraints imposed on atoms in the buffer region, which slow protein motions relative to those in the gas-phase simulation. In addition, energy flow throughout the system might have been less efficient when the Langevin oscillators in the buffer region acted as the heat bath, with a consequent delay in the transfer of kinetic energy to the ammonia copies. In another set of control calculations, the sensitivity of the LES simulations to the number of copies was investigated by placing 10 ammonia molecules in the glutaminase site. As expected, and even in gas-phase calculations, the ligand copies moved through the protein at a rate much slower than that observed in the simulations employing 50 ammonia molecules, with the center of mass of these ligands remaining in the glutaminase site even after 500 ps (Figure 3E). As in previous LES simulations employing 50 copies, however, no ammonia molecules in the interfacial region of the two domains were observed to "leak" into bulk solvent over the period of this simulation. These observations support our initial choice of 50 ammonia copies for obtaining a qualitative picture of the equilibrium distribution within the tunnel with good computational efficiency.

The Ammonia Channel in GPATase Is a Transient Structural Element. X-ray crystallography has revealed a large-scale loop reorganization that takes place after PRPP binding to form the intramolecular tunnel linking the two active sites of the enzyme (*14*). Whether the ammonia tunnel is permanently present in this active conformation is, however, an open question, especially in light of recent calculations that show the importance of side chain dynamics for ammonia translocation in glutamine fructose-5-phosphate amidotransferase

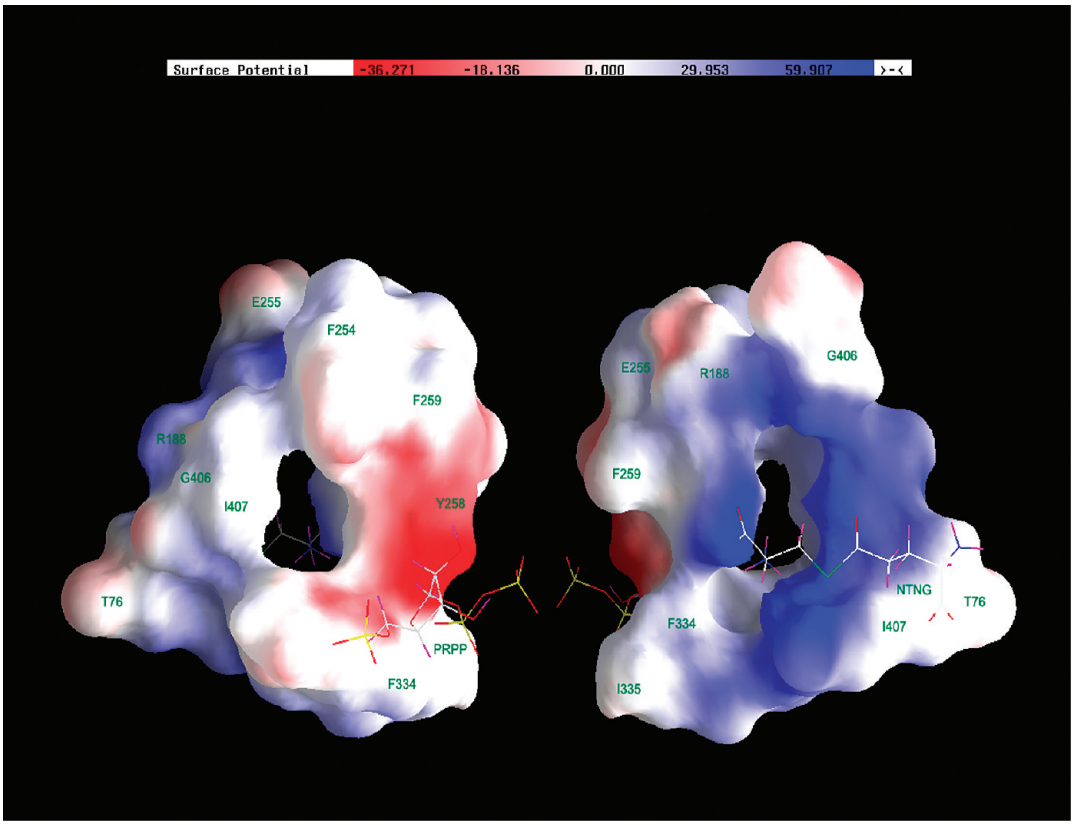

FIGURE 5: Surface representation of the electrostatic potential (MEP) associated with the C-terminal (left) and N-terminal (right) regions of the ammonia tunnel in the thioester−PRPP−GPATase model structure. Note that the interior surface of the tunnel has no significant electrostatic potential, whereas the surfaces in each active site have regions of positive (blue) or negative (red) potential. Atoms in PRPP **3** and the DON adduct are rendered as "stick figures", and residues forming the molecular surface are labeled. Atom coloring: C, white; H, purple; N, blue; O, red; P, yellow; S, green.

(GFAT) (*33*). Snapshots of the LES simulation on the thioester−PRPP−GPATase−NH_3 complex were therefore analyzed to identify intramolecular cavities within the protein using the VOIDOO package (Figure 6) (*67*). These showed that although no contiguous ammonia tunnel was present in the energy-minimized crystal structure (Figure 6A), small cavities (11, 5, and 2 $Å^3$) were observed close to the glutaminase site and the side chains of Ile-335 and Ile-407, respectively. As ammonia molecules became distributed within the putative tunnel during the LES simulation after 25 ps, however, an almost continuous cavity between the glutaminase and synthase active sites was formed (Figure 6D). Similar results were obtained, albeit for snapshots at longer times, for LES calculations on the thioester−PRPP−GPATase−NH_3 complex in a water sphere. Hence, it seems likely that an "open" intramolecular cavity linking the active sites does not exist in the active conformation of GPATase prior to the release of ammonia from glutamine, and local dynamical motions in the protein seem to be required for ammonia to move through the tunnel, which while potentially constituting a significant free energy barrier to ammonia translocation are thermally accessible over short time scales. This finding is consistent with the results of SMD simulations on the motion of ammonia between the two active sites in *E. coli* glucosamine-6-phosphate synthase (*33*), which also showed that local side chain movements, albeit of a small number of residues, were an essential element in permitting the access of ammonia to the synthase site. Recent PMF calculations for movement of ammonia within the large subunit of CPS (*74*) also demonstrate the importance of local side chain motions for reducing relatively high potential energy barriers (7.2 kcal/mol) to intramolecular translocation.

The Ammonia Tunnel in GPATase Discriminates against Ammonium Ion (NH_4^+). In common with other class II amidotransferases (*24*), the GPATase tunnel is lined by side chains that have significant hydrophobic character (Phe-254, Tyr-258, Phe-259, Phe-334, Ile-335, Gly-406, and Ile-407), suggesting that ammonia forms hydrogen bonds with carbonyl groups in the protein backbone (*14*). To determine whether ammonium ion might be transported through the tunnel during catalytic turnover, a stochastic boundary LES calculation was conducted on the GPATase−thioester−PRPP−NH_3 complex, containing 50 copies of NH_4^+ in the glutaminase domain (Figure 3F). In contrast to the cognate simulation with ammonia, ammonium ions were not observed to access the interior of the tunnel but leaked from the protein into bulk solvent after a few picoseconds, with the consequence that no copies remained in the protein after 200 ps. This leakage took place through a hole at the interface of the N- and C-terminal domains defined by the side chains of Thr-76, Asp-408, and Arg-482, and the backbone atoms of Ile-407 and Asp-408 (Figure 4B). Examination of the electrostatic potential on the van der Waals surface of GPATase at the entrance of the tunnel (computed using CHARMM partial atomic charges on the protein atoms) suggests that the barrier arises from a positive potential associated with residues Arg-342, Arg-371, and Arg-482 (Figure 5), which are located a substantial distance from the tunnel entrance.

Free Energy Calculations of Ammonia Translocation in GPATase. Although the LES simulations provided a number of

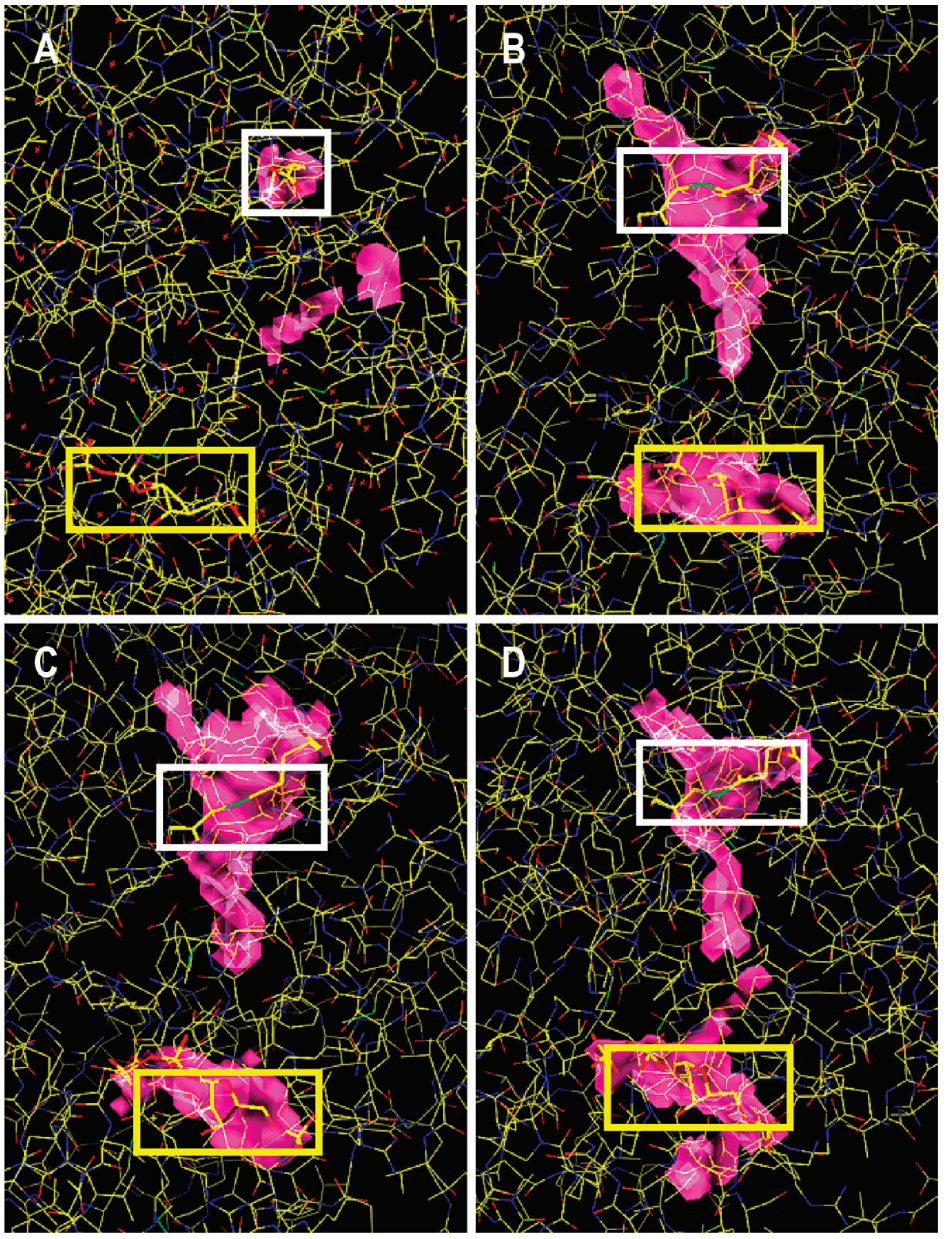

FIGURE 6: (A) Cavities in the geometry-optimized crystal structure of cPRPP **3** bound to DON-modified *E. coli* GPATase (PDB entry 1ECC) and (B−D) development of the ammonia tunnel in the thioester−PRPP−GPATase−NH_3 model complex during the gas-phase LES simulations. Structural snapshots were taken at 5 (B), 10 (C), and 25 ps (D). All intramolecular cavities (indicated by the maroon-colored surface) were calculated using VOIDOO (*65*) and rendered in O (*66*). The glutaminase and synthetase sites in the four GPATase structures, located at each end of the putative ammonia tunnel, are indicated by the white and yellow boxes, respectively. Atom coloring: C, yellow; N, blue; O, red.

qualitative insights into the movement of ammonia between the two active sites in GPATase, we sought to obtain a quantitative picture of (i) the free energy of ammonia when within the tunnel and (ii) the barrier preventing access to ammonium ion. We therefore constructed a series of GPATase−thioester−PRPP−NH_3 structures, containing only a single ammonia molecule (see Materials and Methods), at one of the positions in the final distribution of ammonia copies in the stochastic boundary LES simulation after 28 ps. Each structure was then subjected to an umbrella sampling MD simulation (*65*, *75*) to yield the potential of mean force for ammonia as it moved through the tunnel in the stochastic boundary solvation model. WHAM analysis of the resulting trajectories showed that there is a free energy barrier to ammonia movement of approximately 11 kcal/mol at a distance, δ, of 7 Å from its initial position in the glutaminase site (Figure 7). This barrier appears to be associated with the loss of hydrogen bonds as ammonia moves through the tunnel. For example, when δ = 3.5 Å, ammonia forms a hydrogen bond to the N-terminal amino group of Cys-1, presumably after this moiety has acted as a general base to promote formation of γ-glutamylthioester intermediate **5** (*51*). Moreover, when δ = 4.0 Å, ammonia forms strong hydrogen bonds with the backbone carbonyl oxygens of Tyr-74 and Gly-406, which are located on the opposite sides of the tunnel, thereby "clamping" the small molecule at the entrance. Both of these interactions are absent, however, when δ > 7.0 Å, and the PMF free energy curve becomes relatively flat with small fluctuations within the δ region of 12.0−14.0 Å. The magnitude of the computed free energy barrier for ammonia movement, which is primarily associated with breaking the hydrogen bonds in the glutaminase site, is perhaps surprising if it is believed that tunnels are essentially devices for promoting one-dimensional ligand diffusion (*25*). Our calculated barrier to ammonia translocation,

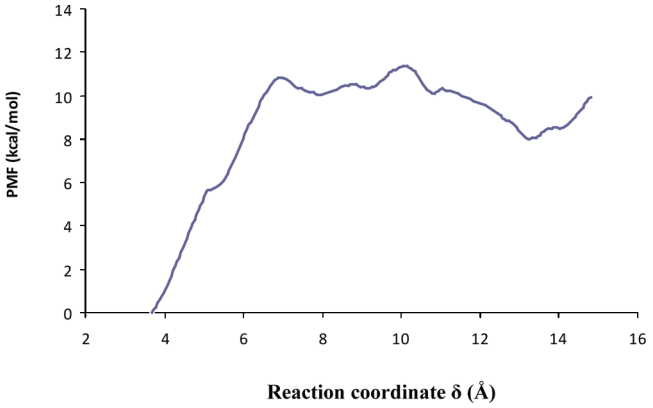

FIGURE 7: Potential of mean force (PMF) profile for the translocation of ammonia through the ammonia tunnel in the thioester−PRPP−GPATase model using the stochastic boundary potential. Distances correspond to those between the nitrogen atom of the ammonia molecule in the center of the *N*th window and the carbonyl carbon of the thioester moiety.

however, is lower than the activation energy calculated from the steady-state turnover number of *E. coli* GPATase. Thus, k_{cat} is approximately 60 s^{-1} at 37 °C (*28*, *47*), which corresponds to an energy of 15.5 kcal/mol assuming a value of 5×10^{12} s^{-1} for the pre-exponential factor (*76*). Furthermore, the ammonia molecule is likely to possess kinetic energy as a result of C−N bond cleavage, which can also be used to overcome the barrier to motion through the tunnel. A second interesting feature of the WHAM calculation is that the free energy of the protein-bound ammonia is higher in the synthetase site (Figure 7). It should be noted, however, that these calculations do not include contributions from the energy released by displacement of pyrophosphate from PRPP and formation of the C−N bond to give 5′-phosphoribosylamine.

Modeling the "Leakiness" of the L415A GPATase Mutant. GPATase exhibits a very high efficiency of coupling glutamine hydrolysis to the synthesis of 5′-phosphoribosylamine (Scheme 1), implying that ammonia is sequestered from bulk solvent during catalytic turnover (*28*). In addition, the enzyme exhibits no significant glutaminase activity in the absence of PRPP (*51*), suggesting the existence of intramolecular interactions that couple PRPP binding with catalysis in the N-terminal site. In studies aimed at probing the function of residues defining the GPATase tunnel, Bera and co-workers reported that replacement of Leu-415 with an alanine residue resulted in a GPATase mutant (L415A) for which the ammonia transfer efficiency was only 30% of that of the wild-type enzyme (*28*). The reason for the decreased efficiency of ammonia translocation was not immediately obvious on the basis of the GPATase−DON−PRPP crystal structure, however, because Leu-415 is not a residue defining the wall of the tunnel (Figure 8).

To investigate the molecular basis of the reduced transfer efficiency in the L415A GPATase mutant, a model of the L415A−thioester−PRPP structure was built using standard graphical manipulation followed by energy minimization. A gas-phase LES simulation was then performed using 50 ammonia copies initially placed in the N-terminal, glutaminase site, with the result that 16 copies leaked from the L415A−thioester−PRPP complex after 50 ps compared to only four copies in the cognate LES simulation of the wild-type enzyme. A detailed analysis of the LES trajectory for the L415A GPATase mutant showed that ammonia was leaking between the N- and C-terminal

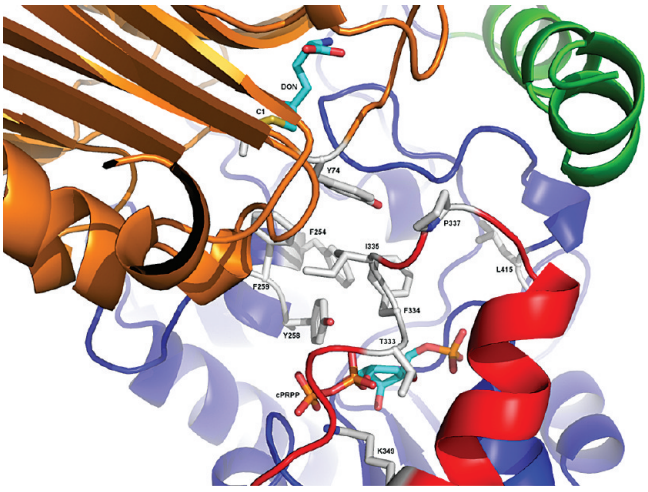

FIGURE 8: View of the intramolecular tunnel in the *E. coli* GPATase−DON−cPRPP complex (PDB entry 1ECC) showing the location of the Leu-415 (L415) side chain relative to the tunnel (defined by residues Tyr-74, Phe-254, Tyr-258, Phe-259, Phe-334, and Ile-335). The cartoon representations of the glutaminase and synthase domains of GPATase are colored orange and blue, respectively, except that peptide segments that undergo conformational changes on ligand binding are colored red (residues 325−354) and green (residues 471−492). DON, cPRPP, and selected residue side chains are shown as sticks. Atom coloring: C, gray; O, red; N, blue; S, yellow. The image was rendered in PYMOL (DeLano Scientific Software LLC, Palo Alto, CA).

domains along a path similar to that observed for the leakage of ammonium ions from wild-type GPATase (Figure 4B). Snapshots of the GPATase−thioester−PRPP−NH_3 and L415A−thioester−PRPP−NH_3 models, taken between 50 and 100 ps in the gas-phase LES simulations, were used to obtain the "average" structure of the two complexes, which were then superimposed so that structural changes associated with the replacement of the Leu-415 side chain could be identified. This comparison showed that replacing Leu-415 with alanine had disrupted the packing of the Thr-76 and Asp-408 side chains and the Ile-407 main chain atoms (Figure S3 of the Supporting Information), resulting in an increase of 1.8 Å in the average C_α−C_α distance of Thr-76 and Asp-408 (Figure 9). Given that Leu-415 is located close to the PRPP binding site, it seemed likely that modification of this side chain was affecting coupled dynamical motions in the protein structure (*72*, *77*, *78*). Evidence for this hypothesis is provided by comparing the root-mean-square (rms) fluctuations averaged over the backbone atoms of each protein residue in MD trajectories calculated for the thioester−ammonia−PRPP complexes of wild-type GPATase and the L415A GPATase mutant (Figure 10). Although many of the backbone motions appear similar in the two model complexes, those of the L415A GPATase mutant show interesting large fluctuations, i.e., values of > 0.8 Å, in regions centered on Leu-190 and Ala-412. The latter residue is spatially adjacent to the side chain of Leu-415, suggesting that mutation of this leucine to alanine impacts hydrophobic contacts in this area of the structure.

Encouraged by these findings in the gas-phase trajectories, we examined solvent effects on the leakiness of the L415A GPATase mutant by repeating the calculations on a solvated L415A−thioester−PRPP−NH_3 model complex. In this case, however, no ammonia copies were observed to leak out of the protein. Instead, up to 20 copies became clustered in a pocket formed by the side chains of Phe-254, Ile-407, Met-409, and Val-460, which was not

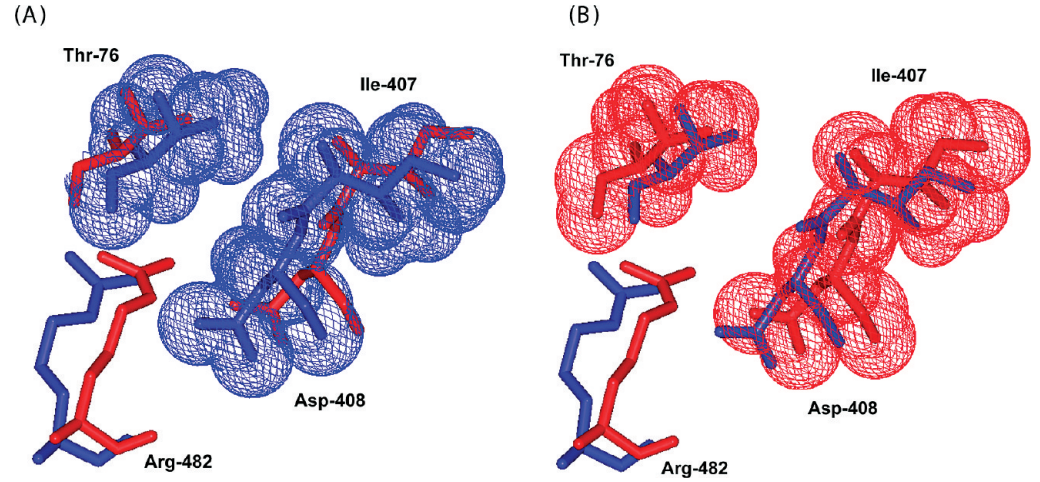

FIGURE 9: Comparison of the average side chain−side chain positions in wild-type GPATase (blue) and the L415A GPATase mutant (red) at the site from which ammonia leaks in the gas-phase LES simulation of the mutant enzyme. The coordinates of atoms in the enzymes correspond to those computed for the average structure computed from snapshots taken between 50 and 100 ps in the LES trajectories of the thioester−PRPP−GPATase−NH_3 and thioester−L415A−GPATase−NH_3 models. (A) Dot representation of the van der Waals surface for atoms in the average structure of wild-type GPATase. (B) Dot representation of the van der Waals surface for atoms in the average structure of the L415A GPATase mutant.

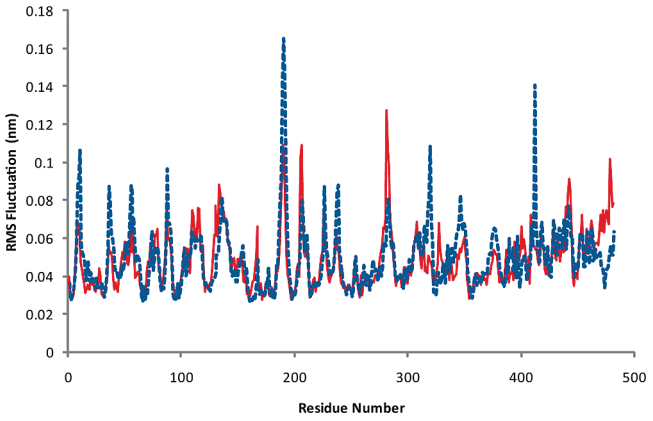

FIGURE 10: Average rms fluctuation of residue backbone atoms during the 50−100 ps time interval in MD simulations for models of the thioester−ammonia−PRPP−wild-type GPATase (red) and thioester−ammonia−PRPP−L415A GPATase mutant (blue) complexes. In both simulations, the ammonia molecule was positioned at the initial position within the glutaminase site used for the LES simulations.

populated in similar stochastic boundary LES simulations on wild-type GPATase. It is likely that this behavior is associated with the absence of low-frequency collective motions in the response functions for atoms in the buffer region (*79*), which are essential for modeling the relatively large conformational changes in this region of the protein that are required for ammonia molecules to leak through the gap between the Thr-76 and Asp-408 side chains.

In summary, the coupling of LES simulation and PMF methods offers a new strategy for examining the translocation of small molecules between active sites in complex enzymes containing multiple active sites, such as glutamine-dependent amidotransferases (*1*, *2*), acetyl-CoA synthase (*80*), and bifunctional aldolase dehydrogenases (*81*). As well as providing quantitative insights into the free energy of the ligand as it moves through the protein, the LES/PMF computational approach provides information about the dynamical properties of the tunnel and the molecular basis for changes in translocation efficiency caused by the site-specific mutations.

The finding that all glutamine-dependent amidotransferases seem to contain intramolecular tunnels linking multiple catalytic sites in their active conformation is, at first sight, remarkable in light of the large variation in the three-dimensional folds of the synthase/synthetase domains in these enzymes and illustrates the extent to which the structural "plasticity" of proteins can be exploited by natural selection (*82*). As a consequence, there are likely to be few general "rules" that govern the length and shape of the tunnels present in amidotransferases, although, in contrast to membrane-bound ammonia transporters (*83*), ammonia translocation in these enzymes does not seem to be driven by differences in electrostatic potential. This is probably because the relatively small lengths of these intramolecular tunnels mean that the time required for ammonia to travel between active sites is an insignificant fraction of that required for the enzyme to complete a single turnover (*25*). On the other hand, all of the other tunnels that have been studied computationally appear to discriminate against transporting ammonium ions between the active sites (*31*, *33*, *34*). This ability of tunnel residues to discriminate between ammonia and ammonium ion presumably ensures that the nitrogen atom is translocated to the synthase/synthetase active site in a chemically reactive form.

ACKNOWLEDGMENT

We thank Alex MacKerell (University of Maryland, College Park, MD) for helpful discussions concerning methods for obtaining and validating force field parameters and for his generous provision of CHARMM parametrization scripts. We also acknowledge access to the computing facilities of the McKnight Brain Institute at the University of Florida.

SUPPORTING INFORMATION AVAILABLE

Details of parametrization methods and parameters, including atom naming conventions (Figure S1) and a comparison of MP2/6-31G(d), RHF/6-31G(d), and CHARMM dihedral potential energies for C1−C−S−C2 and O=C−S−C2 angles in SMTA **6** (Figure S2); full details and validation of new CHARMM27 parameters developed for this study (Tables S1−S5); CHARMM27 force field topology file entries for the thioester

(NTNG), 5′-phosphoribosylpyrophosphate (PRPP), ammonia (NH3), ammonium ion (NH4), and model compounds SMTA **6** and THFP **7** (Charts S1 and S2); CHARMM27 force field file entries for NTNG, PRPP, NH3, NH4, SMTA, and THFP (Chart S3); and time dependence of $C_\alpha - C_\alpha$ distances between residues defining the site of ammonia leakage in the L415A GPATase mutant (Figure S3). This material is available free of charge via the Internet at http://pubs.acs.org.

REFERENCES

1. Zalkin, H. (1993) The amidotransferases. *Adv. Enzymol. Relat. Areas Mol. Biol. 66*, 203–309.
2. Buchanan, J. M. (1973) Amidotransferases. *Adv. Enzymol. Relat. Areas Mol. Biol. 39*, 91–183.
3. Williams, L., Fresquet, V., Santander, P. J., and Raushel, F. M. (2007) The multiple amidation reactions catalyzed by cobyric acid synthetase from *Salmonella typhimurium* are sequential and dissociative. *J. Am. Chem. Soc. 129*, 294–295.
4. Wojcik, M., Seidle, H. F., Bieganowski, P., and Brenner, C. (2006) Glutamine-dependent NAD^+ synthetase: How a two-domain, three-substrate enzyme avoids waste. *J. Biol. Chem. 281*, 33395–33402.
5. Fitzpatrick, T. B., Amrhein, N., Kappes, B., Macheroux, F., Tews, I., and Raschle, T. (2007) Two independent routes of *de novo* vitamin B6 biosynthesis: Not that different after all. *Biochem. J. 407*, 1–13.
6. Kappock, T. J., Ealick, S. E., and Stubbe, J. (2000) Modular evolution of the purine biosynthetic pathway. *Curr. Opin. Chem. Biol. 4*, 567–572.
7. Evans, D. R., and Guy, H. I. (2004) Mammalian pyrimidine biosynthesis: Fresh insights into an ancient pathway. *J. Biol. Chem. 279*, 33035–33038.
8. Richards, N. G. J., and Kilberg, M. S. (2006) Asparagine synthetase chemotherapy. *Annu. Rev. Biochem. 75*, 629–654.
9. Ibba, M., Becker, H. D., Stathopoulos, C., Tumbula, D. L., and Söll, D. (2000) The adaptor hypothesis revisited. *Trends Biochem. Sci. 25*, 311–316.
10. Klem, T. J., and Davisson, V. J. (1993) Imidazole glycerol phosphate synthase: The glutamine transferase in histidine biosynthesis. *Biochemistry 32*, 5177–5186.
11. Vanoni, M. A., and Curti, B. (2005) Structure-function studies on the iron-sulfur flavoenzyme glutamate synthase: An unexpectedly complex self-regulated enzyme. *Arch. Biochem. Biophys. 433*, 193–211.
12. Teplyakov, A., Leriche, C., Obmolova, G., Badet, B., and Badet-Denisot, M.-A. (2002) From Lobry de Bruyn to enzyme-catalyzed ammonia channeling: Molecular studies of D-glucosamine-6P synthase. *Nat. Prod. Rep. 19*, 60–69.
13. Thoden, J. B., Holden, H. M., Wesenberg, G., Raushel, F. M., and Rayment, I. (1997) Structure of carbamoyl phosphate synthetase: A journey of 96 Å from substrate to product. *Biochemistry 36*, 6305–6316.
14. Krahn, J. M., Kim, J. H., Burns, M. R., Parry, R. J., Zalkin, H., and Smith, J. L. (1997) Coupled formation of an amidotransferase interdomain ammonia channel and a phosphoribosyltransferase active site. *Biochemistry 36*, 11061–11068.
15. Larsen, T. M., Boehlein, S. K., Schuster, S. M., Richards, N. G. J., Thoden, J. B., Holden, H. M., and Rayment, I. (1999) Three-dimensional structure of *Escherichia coli* asparagine synthetase B: A short journey from substrate to product. *Biochemistry 38*, 16146–16157.
16. Chauduri, B. N., Lange, S. C., Myers, R. S., Chittur, S. V., Davisson, V. J., and Smith, J. L. (2001) Crystal structure of imidazole glycerol phosphate synthase: A tunnel through a $(\beta/\alpha)_8$ barrel joins two active sites. *Structure 9*, 987–997.
17. van den Heuvel, R. H. H., Svergun, D. I., Petoukhov, M. V., Coda, A., Curti, B., Ravasio, S., Vanoni, M. A., and Mattevi, A. (2003) The active conformation of glutamate synthase and its binding to ferredoxin. *J. Mol. Biol. 330*, 113–128.
18. Anand, R., Hoskins, A. A., Stubbe, J., and Ealick, S. E. (2004) Domain organization of *Salmonella typhimurium* formylglycinamide amidotransferase revealed by X-ray crystallography. *Biochemistry 43*, 10328–10342.
19. Endrizzi, J. A., Kim, H., Anderson, P. M., and Baldwin, E. P. (2004) Crystal structure of *Escherichia coli* cytidine triphosphate synthetase, a nucleotide-regulated glutamine amidotransferase/ATP-dependent amidoligase fusion protein of anticancer and antiparasitic drug targets. *Biochemistry 43*, 6447–6463.
20. Strohmeier, M., Raschle, T., Mazurkiewicz, J., Rippe, K., Sinning, I., Fitzpatrick, T. B., and Tews, I. (2006) Structure of a bacterial pyridoxal 5′-phosphate synthase complex. *Proc. Natl. Acad. Sci. U. S.A. 103*, 19284–19289.
21. Mouilleron, S., Badet-Denisot, M.-A., and Golinelli-Pimpaneau, B. (2006) Glutamine binding opens the ammonia channel and activates glucosamine-6P synthase. *J. Biol. Chem. 281*, 4404–4412.
22. Oshikane, H., Sheppard, K., Fukai, S., Nakamura, Y., Ishitani, R., Numata, T., Sherrer, R. L., Feng, L., Schmitt, E., Panvert, M., Blanquet, S., Mechulam, Y., Söll, D., and Nureki, O. (2006) Structural basis of RNA-dependent recruitment of glutamine to the genetic code. *Science 312*, 1950–1954.
23. Weeks, A., Lund, L., and Raushel, F. M. (2006) Tunneling of intermediates in enzyme-catalyzed reactions. *Curr. Opin. Chem. Biol. 10*, 465–472.
24. Raushel, F. M., Thoden, J. B., and Holden, H. M. (2003) Enzymes with molecular tunnels. *Acc. Chem. Res. 36*, 539–548.
25. Huang, X., Holden, H. M., and Raushel, F. M. (2001) Channeling of substrates and intermediates in enzyme-catalyzed reactions. *Annu. Rev. Biochem. 70*, 149–180.
26. Huang, X., and Raushel, F. M. (2000) An engineered blockage within the ammonia tunnel in carbamoyl phosphate synthetase prevents the use of glutamine as a substrate but not ammonia. *Biochemistry 39*, 3240–3247.
27. Thoden, J. B., Huang, X., Raushel, F. M., and Holden, H. M. (2002) Carbamoyl phosphate synthetase: Creation of an escape route for ammonia. *J. Biol. Chem. 277*, 39722–39727.
28. Bera, A. K., Smith, J. L., and Zalkin, H. (2000) Dual role for the glutamine phosphoribosyl-pyrophosphate amidotransferase ammonia channel: Interdomain signaling and intermediate channeling. *J. Biol. Chem. 275*, 7975–7979.
29. Mullins, L. S., and Raushel, F. M. (1999) Channeling of ammonia through the intermolecular tunnel contained within carbamoyl phosphate synthetase. *J. Am. Chem. Soc. 121*, 3803–3804.
30. Li, K. K., Beeson, W. T., IV, Ghiviriga, I., and Richards, N. G. J. (2007) A gHMQC-based assay for investigating ammonia channeling: Application to studies of glutamine-dependent asparagine synthetase. *Biochemistry 46*, 4840–4849.
31. Amaro, R. E., Myers, R. S., Davisson, V. J., and Luthey-Schulten, Z. A. (2005) Structural elements in IGP synthase exclude water to optimize ammonia transfer. *Biophys. J. 89*, 475–487.
32. Amaro, R., and Luthey-Schulten, Z. (2004) Molecular dynamics simulations of substrate channeling through an α-β barrel protein. *Chem. Phys. 307*, 147–155.
33. Floquet, N., Mouilleron, S., Daher, R., Maigret, B., Badet, B., and Badet-Denisot, M.-A. (2007) Ammonia channeling in bacterial glucosamine-6-phosphate synthase (Glms): Molecular dynamics simulations and kinetic studies of protein mutants. *FEBS Lett. 581*, 2981–2987.
34. Fan, Y., Lund, L., Yang, L., Raushel, F. M., and Gao, Y.-Q. (2008) The mechanism for the transport of ammonia within the carbamoyl phosphate synthetase determined by molecular dynamics simulations. *Biochemistry 47*, 295–2944.
35. Amaro, R. E., Sethi, A., Myers, R. S., Davisson, V. J., and Luthey-Schulten, Z. A. (2007) A network of conserved interactions regulates the allosteric signal in a glutamine amidotransferase. *Biochemistry 46*, 2156–2173.
36. Myers, R. S., Amaro, R. E., Luthey-Schulten, Z. A., and Davisson, V. J. (2005) Reaction coupling through interdomain contacts in imidazole glycerol phosphate synthase. *Biochemistry 44*, 11974–11985.
37. Park, S., Khalili-Araghi, F., Tajkhorshid, E., and Schulten, K. (2003) Free energy calculation from steered molecular dynamic simulations using Jarzynski's equation. *J. Chem. Phys. 119*, 3559–3566.
38. Verkhivker, G., Elber, R., and Nowak, W. (1992) Locally enhanced sampling in free energy calculations: Application of mean field approximation to accurate calculation of free energy differences. *J. Chem. Phys. 97*, 7838–7841.
39. Czerminski, R., and Elber, R. (1991) Computational studies of ligand diffusion in globins: I. Leghemoglobin. *Proteins: Struct., Funct., Genet. 10*, 70–80.
40. Norberg, J., and Nilsson, L. (2003) Advances in biomolecular simulations: Methodology and recent applications. *Q. Rev. Biophys. 36*, 257–306.
41. Roux, B. (1995) The calculation of the potential of mean force using computer simulations. *Comput. Phys. Commun. 91*, 275–282.
42. Martínez, L., Sonoda, M. T., Webb, P., Baxter, J. D., Skaf, M. S., and Polikarpov, I. (2005) Molecular dynamics simulations reveal multiple pathways of ligand dissociation from thyroid hormone receptors. *Biophys. J. 89*, 2011–2023.
43. Sonoda, M. T., Martínez, L., Webb, P., Skaf, M. S., and Polikarpov, I. (2008) Ligand dissociation from estrogen receptor is mediated by

receptor dimerization: Evidence from molecular dynamics simulations. *Mol. Endocrinol. 22*, 1565–1578.
44. Roitberg, A., and Elber, R. (1991) Modeling side chains in peptides and proteins: Application of the locally enhanced sampling and simulated annealing methods to find minimum energy conformations. *J. Chem. Phys. 95*, 9277–9287.
45. Smith, J. L., Zaluzec, E. J., Wery, J.-P., Niu, L., Switzer, R. L., Zalkin, H., and Satow, Y. (1994) Structure of the allosteric regulatory enzyme of purine biosynthesis. *Science 264*, 1427–1433.
46. Bera, A. K., Chen, S., Smith, J. L., and Zalkin, H. (1999) Interdomain signaling in glutamine phosphoribosylpyrophosphate amidotransferase. *J. Biol. Chem. 274*, 36498–36504.
47. Chen, S., Burgner, J. W., Krahn, J. M., Smith, J. L., and Zalkin, H. (1999) Tryptophan fluorescence monitors multiple conformational changes required for glutamine phosphoribosylpyrophosphate amidotransferase interdomain signaling and catalysis. *Biochemistry 38*, 11659–11669.
48. Parry, R. J., Burns, M. R., Jiralerspong, S., and Alemany, L. (1997) Synthesis of (+)-(1*S*)-1-pyrophosphoryl-(2*R*,3*R*)-2,3-dihydroxy-(4*S*)-4-(phosphoryloxymethyl)cyclopentane, a stable, optically active carbocyclic analog of 5-phosphoribosyl-1-pyrophosphate (PRPP). *Tetrahedron 53*, 7077–7088.
49. Parry, R. J., and Haridas, K. (1993) Synthesis of 1α-pyrophosphoryl-2α,3α-dihydroxy-4*β*-cyclopentanemethanol-5-phosphate, a carbocyclic analog of 5-phosphoribosyl-1-pyrophosphate (PRPP). *Tetrahedron Lett. 34*, 7013–7016.
50. Jayaram, H. N., Cooney, D. A., Milman, H. A., Homan, E. R., and Rosenbluth, R. J. (1976) DON, CONV and DONV. I. Inhibition of L-asparagine synthetase *in vitro*. *Biochem. Pharmacol. 25*, 1571–1582.
51. Zalkin, H., and Smith, J. L. (1998) Enzymes utilizing glutamine as an amide donor. *Adv. Enzymol. Relat. Areas Mol. Biol. 72*, 72–144.
52. Richards, N. G. J., and Schuster, S. M. (1998) Mechanistic issues in asparagine synthetase catalysis. *Adv. Enzymol. Relat. Areas Mol. Biol. 72*, 145–198.
53. Brooks, B. R., Bruccoleri, R. E., Olafson, B. D., States, D. J., Swaminathan, S., and Karplus, M. (1983) CHARMM: A program for macromolecular energy minimization, and dynamics calculations. *J. Comput. Chem. 4*, 187–217.
54. MacKerell, A. D., Jr., Bashford, D., Bellott, M., Dunbrack, R. L., Jr., Evanseck, J. D., Field, M. J., Fischer, S., Gao, J., Guo, H., Ha, S., Joseph-McCarthy, D., Kuchnir, L., Kuczera, K., Lau, F. T. K., Mattos, C., Michnick, S., Ngo, T., Nguyen, D. T., Prodhom, B., Reiher, W. E., III, Roux, B., Schlenkrich, M., Smith, J. C., Stote, R., Straub, J., Watanabe, M., Wiórkiewicz-Kuczera, J., Yin, D., and Karplus, M. (1998) All-atom potential for molecular modeling and dynamics studies of proteins. *J. Phys. Chem. B 102*, 3586–3616.
55. Foloppe, N., and MacKerell, A. D., Jr. (2000) All-atom empirical force field for nucleic acids: 1. Parameter optimization based on small molecule and condensed phase macromolecular target data. *J. Comput. Chem. 21*, 86–104.
56. MacKerell, A. D., Jr. (2004) Empirical force field for biological macromolecules: Overview and issues. *J. Comput. Chem. 25*, 1584–1604.
57. Schnizer, H. G., Boehlein, S. K., Stewart, J. D., Richards, N. G. J., and Schuster, S. M. (1999) Formation and isolation of a covalent intermediate during the glutaminase reaction of a class II amidotransferase. *Biochemistry 38*, 3677–3682.
58. Elber, R., and Karplus, M. (1990) Enhanced sampling in molecular dynamics: Use of the time-dependent Hartree approximation for a simulation of carbon monoxide diffusion through myoglobin. *J. Am. Chem. Soc. 112*, 9161–9175.
59. Hoover, W. G. (1985) Canonical dynamics: Equilibrium phase space distributions. *Phys. Rev. A 31*, 1695–1697.
60. Nosé, S. J. (1984) A unified formulation of the constant temperature molecular dynamics methods. *J. Chem. Phys. 81*, 511–519.
61. van Gunsteren, W. F., and Berendsen, H. J. C. (1977) Algorithms for macromolecular dynamics and constraint dynamics. *Mol. Phys. 34*, 1311–1327.
62. Jorgensen, W. L., Chandrasekhar, J., Madura, J., Impey, R. W., and Klein, M. L. (1983) Comparison of simple potential functions for simulating liquid water. *J. Chem. Phys. 79*, 926–935.
63. Brooks, C. L., III, and Karplus, M. (1989) Solvent effects on protein motion and protein effects on solvent motion. *J. Mol. Biol. 208*, 159–181.
64. Brooks, C. L., III, Brünger, A., and Karplus, M. (1985) Active site dynamics in protein molecules: A stochastic boundary molecular dynamics approach. *Biopolymers 24*, 843–865.
65. Kottalam, J., and Case, D. A. (1988) Dynamics of ligand escape from the heme pocket of myoglobin. *J. Am. Chem. Soc. 110*, 7690–7697.
66. Kumar, S., Rosenberg, J. M., Bouzida, D., Swendsen, R. H., and Kollman, P. A. (1995) Multi-dimensional free energy calculations using the weighted histogram analysis method. *J. Comput. Chem. 16*, 1339–1350.
67. Kleywegt, G. J., and Jones, T. A. (1994) Detection, delineation, measurement and display of cavities in macromolecular structures. *Acta Crystallogr. D50*, 178–185.
68. Jones, T. A., Zou, J. Y., Cowan, S. W., and Kjeldgaard, M. (1991) Improved methods for building protein models in electron density maps and the location of errors in these models. *Acta Crystallogr. A47*, 110–119.
69. Kleywegt, G. J., and Jones, T. A. (1996) xdlMAPMAN and xdlDATAMAN. Programs for reformatting, analysis and manipulation of biomacromolecular electron density maps and reflection data sets. *Acta Crystallogr. D52*, 826–828.
70. Nicholls, A., Sharp, K. A., and Honig, B. (1991) Protein folding and association: Insights from the interfacial and thermodynamic properties of hydrocarbons. *Proteins: Struct., Funct., Genet. 11*, 281–296.
71. Benkovic, S. J., Hammes, G. G., and Hammes-Schiffer, S. (2008) Free energy landscape of enzyme catalysis. *Biochemistry 47*, 3317–3321.
72. Boehr, D. D., Dyson, H. J., and Wright, P. E. (2006) An NMR perspective on enzyme dynamics. *Chem. Rev. 106*, 3055–3079.
73. Olsson, M. H. M., Parson, W. W., and Warshel, A. (2006) Dynamical contributions to enzyme catalysis: Critical tests of a popular hypothesis. *Chem. Rev. 106*, 1737–1756.
74. Fan, Y., Lund, L., Shao, Q., Gao, Y.-Q., and Raushel, F. M. (2009) A combined theoretical and experimental study of the ammonia tunnel in carbamoyl phosphate synthetase. *J. Am. Chem. Soc. 131*, 10211–10219.
75. Beveridge, D. L., and DiCapua, F. M. (1989) Free energy via molecular simulation: Applications to chemical and biomolecular systems. *Annu. Rev. Biophys. Biophys. Chem. 18*, 431–492.
76. Himo, F. (2006) Quantum chemical modeling. *Theor. Chem. Acc. 116*, 232–240.
77. Radkiewicz, J. L., and Brooks, C. L., III (2000) Protein dynamics in enzymatic catalysis: Exploration of dihydrofolate reductase. *J. Am. Chem. Soc. 122*, 225–231.
78. Karplus, M. (2000) Aspects of protein reaction dynamics: Deviations from simple behavior. *J. Phys. Chem. B 104*, 11–27.
79. Brooks, C. L., III, Brunger, A., and Karplus, M. (1985) Active site dynamics in protein molecules. A stochastic boundary molecular dynamics approach. *Biopolymers 24*, 843–865.
80. Maynard, E. L., and Lindahl, P. A. (2001) Catalytic coupling of the active sites in acetyl-CoA synthase, a bifunctional CO channeling enzyme. *Biochemistry 40*, 13262–13267.
81. Manjasetty, B. A., Powlowski, J., and Vrielink, A. (2003) Crystal structure of a bifunctional aldolase-dehydrogenase: Sequestering a reactive and volatile intermediate. *Proc. Natl. Acad. Sci. U.S.A. 100*, 6992–6997.
82. Kinch, L. N., and Grishin, N. V. (2002) Evolution of protein structures and functions. *Curr. Opin. Struct. Biol. 12*, 400–408.
83. Javelle, A., Lupo, D., Ripoche, P., Fulford, T., Merrick, M., and Winkler, F. K. (2008) Substrate binding, deprotonation, and, selectivity at the periplasmic entrance of the *Escherichia coli* ammina channel AmtB. *Proc. Natl. Acad. Sci. U.S.A. 105*, 5040–5045.